# Sensitivity of Phytoplankton Primary Production Estimates to Available Irradiance Under Heterogeneous Sea Ice Conditions

Philippe Massicotte, Ilka Peeken, Christian Katlein, Hauke Flores, Yannick Huot, Giulia Castellani, Stefanie Arndt, Benjamin Lange, Jean-éric Tremblay, Marcel Babin

JGR Oceans

RESEARCH ARTICLE
10.1029/2019JC015007

# Sensitivity of Phytoplankton Primary Production Estimates to Available Irradiance Under Heterogeneous Sea Ice Conditions

**Philippe Massicotte[1,2], Ilka Peeken[3], Christian Katlein[1,3], Hauke Flores[3], Yannick Huot[4], Giulia Castellani[3], Stefanie Arndt[3], Benjamin A. Lange[3,5], Jean-Éric Tremblay[1,2], and Marcel Babin[1,2]**

[1]Takuvik Joint International Laboratory (UMI 3376)—Université Laval (Canada) & Centre National de la Recherche Scientifique (France), Québec, Québec, Canada, [2]Québec-Océan et département de biologie, Université Laval, Québec, Québec, Canada, [3]Alfred-Wegener-Institut Helmholtz-Zentrum für Polar- und Meeresforschung, Bremerhaven, Germany, [4]Département de géomatique appliquée, Université de Sherbrooke, Sherbrooke, Québec, Canada, [5]Freshwater Institute, Fisheries and Oceans Canada, Winnipeg, Manitoba, Canada

**Key Points:**
- Phytoplankton primary production under heterogeneous sea ice is spatially highly variable
- Transmittance sampled with profiling platforms improves the accuracy of primary production estimates
- Upscaling estimates at larger spatial scales using satellite sea ice concentration further reduced the error

**Correspondence to:**
P. Massicotte,
philippe.massicotte@takuvik.ulaval.ca

**Citation:**
Massicotte, P., Peeken, I., Katlein, C., Flores, H., Huot, Y., Castellani, G., et al. (2019). Sensitivity of phytoplankton primary production estimates to available irradiance under heterogeneous sea ice conditions. *Journal of Geophysical Research: Oceans*, *124*, 5436–5450. https://doi.org/10.1029/2019JC015007

Received 28 JAN 2019
Accepted 21 JUN 2019
Accepted article online 30 JUN 2019
Published online 4 AUG 2019

**Abstract** The Arctic ice scape is composed by a mosaic of ridges, hummocks, melt ponds, leads, and snow. Under such heterogeneous surfaces, drifting phytoplankton communities are experiencing a wide range of irradiance conditions and intensities that cannot be sampled representatively using single-location measurements. Combining experimentally derived photosynthetic parameters with transmittance measurements acquired at spatial scales ranging from hundreds of meters (using a remotely operated vehicle, ROV) to thousands of meters (using a surface and underice trawl, SUIT), we assessed the sensitivity of water column primary production estimates to multiscale underice light measurements. Daily primary production calculated from transmittance from both the ROV and the SUIT ranged between 0.004 and 939 $mgC \cdot m^{-2} \cdot day^{-1}$. Upscaling these estimates at larger spatial scales using satellite-derived sea ice concentration reduced the variability by 22% (0.004–731 $mgC \cdot m^{-2} \cdot day^{-1}$). The relative error in primary production estimates was two times lower when combining remote sensing and in situ data compared to ROV-based estimates alone. These results suggest that spatially extensive in situ measurements must be combined with large-footprint sea ice coverage sampling (e.g., remote sensing, aerial imagery) to accurately estimate primary production in ice-covered waters. Also, the results indicated a decreasing error of primary production estimates with increasing sample size and the spatial scale at which in situ measurements are performed. Conversely, existing estimates of spatially integrated phytoplankton primary production in ice-covered waters derived from single-location light measurements may be associated with large statistical errors. Considering these implications is important for modeling scenarios and interpretation of existing measurements in a changing Arctic ecosystem.

## 1. Introduction

The Arctic Ocean (AO) icescape is a mosaic composed of sea ice, snow, leads, melt ponds, and open water. During the last decades, this AO icescape has been undergoing major changes, including a reduction in extent and thickness (Meier et al., 2014) and an increased drift speed (Kwok et al., 2013). A greater frequency of storm events is also making this icescape more prone to deformation (Itkin et al., 2017) and promotes lead formation. Because of the surface heterogeneity of the AO icescape, light transmittance can be highly variable in space, even over short distances (Hancke et al., 2018; Katlein et al., 2015; Nicolaus et al., 2013). For example, Perovich et al. (1998) showed that sea ice and snow transmittance at 440 nm could vary by a factor of two over horizontal distances of 25 m. The relative contribution of various sea ice features to underice light variability depends on the spatial scale under consideration and has significant implications for their application in physical and ecological studies and also determines the context in which results can be interpreted. For instance, at small scales (<100 m), local features such as melt ponds and leads have a strong influence on light penetration (Frey et al., 2011; Katlein et al., 2016; Massicotte et al., 2018). At larger scales (>100 m), it was argued that the variability of transmittance is mainly controlled by sea ice thickness (Katlein, 2015).

Because phytoplankton is exposed to a highly variable light regime while drifting under a spatially heterogeneous and sometimes dynamic sea ice surface, single-location irradiance measurements are not

representative of the average irradiance experienced by phytoplankton over a large area (Katlein et al., 2016; Lange et al., 2017). This is why traditional primary production estimated using in situ incubations at single locations with seawater samples inoculated with $^{14}C$ or $^{13}C$ are also not appropriate, because they reflect primary production under local light conditions, which is not representative of the range of irradiance experienced by drifting phytoplankton. A better option consists in calculating primary production using daily time series of incident irradiance, sea ice transmittance, and in-water vertical attenuation coefficients, combined with photosynthetic parameters determined using photosynthesis versus irradiance curves ($P$ vs. $E$ curves) measured with incubations of seawater samples inoculated with $^{14}C$. However, this approach requires an adequate description of the underwater light field, which cannot be characterized using single-location measurements in a spatially heterogeneous sea ice surface. To better estimate primary production of phytoplankton under sea ice, the large-area variability in the light field should be adequately captured.

One major challenge in obtaining adequate irradiance estimates under spatially heterogeneous sea ice is that observations are often limited to time-consuming single-location measurements made through boreholes. To overcome this limitation, different underwater technologies have been developed to study the spatial variability of light transmission under spatially heterogeneous sea ice surfaces. For the last decade, radiometers have been attached to remotely operated vehicles (ROV). Small-sized ROVs can be deployed through relatively small holes (<2 m) to cover areas in the order of a few hundred meters (Ambrose et al., 2005; Katlein et al., 2015, 2017; Lund-Hansen et al., 2018; Nicolaus et al., 2010). Navigating directly under sea ice, ROVs allow covering various types of sea ice, such as newly formed, ponded and snow-covered sea ice, as well as pressure ridges (Katlein et al., 2017). More recently, radiometers have been attached to the surface and underice trawl (SUIT). The SUIT is a trawl developed for sampling mesofauna and macrofauna in the ice-water interface layer, allowing for greater spatial coverage on the order of a few kilometers (Flores et al., 2012; Lange et al., 2016, 2017).

In a recent study, Massicotte et al. (2018) showed that under spatially heterogeneous sea ice and snow surfaces, propagating measured surface downward irradiance just below sea ice $E_d(0^-)$ into the water column using upward attenuation coefficient ($K_{L_u}$) calculated from radiance profiles is a better choice compared to the traditional downward vertical attenuation coefficient ($K_{E_d}$), because it is less influenced by surface heterogeneity. However, while the method allows propagation of irradiance to depth from $E_d(0^-)$ more accurately, estimation of representative $E_d(0^-)$ remains difficult. Both ROV and SUIT aim to better describe the horizontal variability of $E_d(0^-)$ under heterogeneous sea ice. Since these technologies are designed to operate at different scales and in different conditions, they are likely to provide complementary information on the light regime experienced by drifting phytoplankton.

In this study, we investigated the spatial variability of light transmittance measured from these two devices and combined them with satellite-derived sea ice concentrations. We further used these transmittance data measured at different horizontal spatial scales to quantify how they influence primary production estimates derived from photosynthetic parameters. The main objective was to determine if combining multiscale underice transmittance observations with photosynthetic parameters, which are derived under a range of different irradiances, could provide adequate estimates of primary production under sea ice. This study further aimed at addressing the sensitivity of the phytoplankton to heterogeneous irradiance. It provides new guidance on how to derive more representative primary production estimates under a heterogeneous and changing icescape.

## 2. Materials and Methods

### 2.1. Sampling Campaign and Study Sites

Process studies on biological productivity and ecosystem interactions were carried out north of Spitsbergen during the international Transitions in the Arctic Seasonal Sea Ice Zone (TRANSSIZ) expedition aboard the RV *Polarstern* (PS92, ARK-XXIX/1) between 19 May and 26 June 2015. In total, eight process studies (stations 19, 27, 31, 32, 39, 43, 46, and 47) were carried out where the ship was anchored to an ice floe, typically for 36 hr (Figure 1 and Table 1). While the ship drifted anchored to the ice floe on the portside of the ship, winch-operated instruments were deployed in the open water on the starboardside. Water samples for $P$ versus $E$ curves were collected using a conductivity-temperature-depth (CTD)/Rosette. On-ice station work included the deployment of a small observation class ROV under the ice to investigate the small-scale

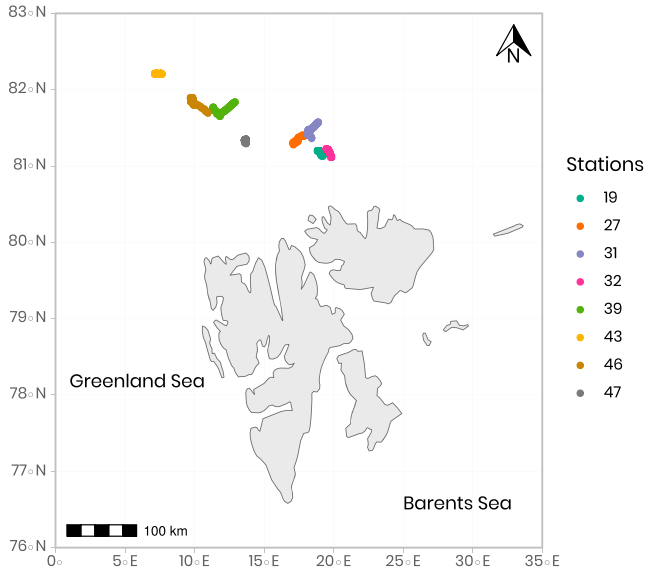


**Figure 1.** Locations of the ice stations sampled during the TRANSSIZ expedition north of Svalbard. The dots reflect the drift of the ship while anchored to an ice floe.

irradiance variability. Prior to arriving or directly after leaving each ice station, the SUIT was deployed for larger-scale characterization of the underice irradiance field. Due to instrument failure, no SUIT data are available for station 32.

### 2.2. Sea Ice and Snow Thicknesses and Sea Ice Concentrations

Ground-based multifrequency electromagnetic induction soundings from a GEM-2 (Geophex Ltd., Raleigh, NC, USA) were used to measure the total thickness of both sea ice and snow following the ROV survey grid. The snow thickness during GEM-2 surveys was measured with a Snow-Hydro Magna Probe instrument (SnowHydro LLC, Fairbanks, Alaska, USA) with a precision of 3 mm (Sturm et al., 2006). The instrument was inserted in the snow approximately every 2 m. The combined GEM-2 and Magna Probe measurements started immediately after the ROV light transmission measurements were finished to ensure that the snow surface was undisturbed. Sea ice thickness was calculated as the difference between total snow and ice thickness and snow depth. The snow thickness displayed in Table 1 is based on ice cores sampled at each station. Sea ice concentration (SIC) data were obtained from www.meereisportal.de and processed according to algorithms in Spreen et al. (2008).

### 2.3. Underwater Light Measurements

#### 2.3.1. ROV Measurements

ROV observations were taken using similar procedures as presented in Nicolaus and Katlein (2013) and Katlein et al. (2017) using a V8 Sii ROV (Ocean Modules, Atvidaberg, Sweden) and RAMSES-ACC-VIS (TriOs

**Table 1**
*Physical Characteristics of the Seven Sations Sampled During the TRANSSIZ Campaign of 2015*

| Station | Date | Latitude (N) | Longitude (E) | Water depth (m) | Snow thickness (m) | SIC (%) | $K_d$(PAR) ($m^{-1}$) |
|---|---|---|---|---|---|---|---|
| 19 | 2015-5-28 | 81.17 | 19.13 | −377 | 0.20 | 71 | 0.59 |
| 27 | 2015-5-31 | 81.39 | 17.59 | −876 | 0.27 | 96 | 0.25 |
| 31 | 2015-6-3 | 81.62 | 19.43 | −1,963 | 0.36 | 97 | 0.22 |
| 39 | 2015-6-11 | 81.92 | 13.46 | −1,589 | 0.18 | 99 | 0.15 |
| 43 | 2015-6-15 | 82.21 | 7.59 | −804 | 0.20 | 100 | 0.14 |
| 46 | 2015-6-17 | 81.89 | 9.73 | −906 | 0.10 | 100 | 0.07 |
| 47 | 2015-6-19 | 81.35 | 13.61 | −2,171 | 0.14 | 100 | 0.17 |

*Note*. Dates are formatted as year-month-day.

GmbH, Rastede, Germany) spectroradiometers mounted both on the ROV and in a fixed location above the sea ice surface. The ROV was deployed through a hole drilled through the ice at a distance of more than 300 m from the ship. Optical measurements were performed along two perpendicular 100-m transects and in a push-broom pattern over a 100-m by 100-m area. Spectral downward irradiance ($E_d$, W/m$^2$) between 320 and 950 nm was recorded above and below the surface to calculate spectral light transmittance as the ratio of irradiance transmitted through the snow/ice to incident irradiance. The sensors were triggered in *burst* mode with the sensors acquiring data as fast as possible. To account for ROV movement, all data with ROV roll and pitch angles larger than 10° and with a distance of more than 3-m depth to the ice cover were rejected from further analysis. To account for light attenuation between the ice-water interface and the sensor, an exponential function was used to obtain the transmission at the ice-water interface:

$$T(z_{\text{int}}) = \frac{T(z)}{e^{-K_{E_d}(\text{PAR}) \times -z}} \tag{1}$$

where $T(z_{\text{int}})$ is the transmittance of the ice and snow at the ice-water interface, $T(z)$ the photosynthetically active radiation (PAR) transmittance measured by the ROV at depth $z$ (m) and $K_{E_d}$(PAR) is the downward diffuse attenuation coefficient of PAR (m$^{-1}$) calculated from $E$(PAR) vertical profiles (equation (2)). At each station, at some point during the survey, the ROV measured a vertical irradiance profile between the surface and at least 20-m depth. Photosynthetically available radiation downwelling irradiance ($E$(PAR, z), µmol·m$^{-2}$·s$^{-1}$), was calculated as follows:

$$E(\text{PAR}, z) = \frac{1}{hc}\frac{1}{N}\int_{400}^{700} \lambda E_d(\lambda, z)\mathrm{d}\lambda \tag{2}$$

where $h$ is Planck's constant, describing the energy content of quanta ($6.623 \times 10^{-34}$ J s), $c$ is the constant speed of light (299,792,458 m/s), $N$ is Avogadro's number ($6.022 \times 10^{23}$ mol$^{-1}$), and $E_d(\lambda, z)$ is the measured irradiance at wavelength $\lambda$ (nm) at depth $z$. Conversion from mol to µmol has been done using a factor of $1 \times 10^6$. Note that planar, $\mathring{E}$(PAR), was converted to scalar irradiance, $\mathring{E}$(PAR), using a conversion factor of 1.2 (Toole et al., 2003). For each vertical $\mathring{E}$(PAR) profile, $K_{\mathring{E}_d}$(PAR)was calculated by fitting the following equation to the measured irradiance data:

$$\mathring{E}(\text{PAR}, z) = \mathring{E}(\text{PAR}, z_{\text{int}})e^{K_{\mathring{E}_d}(\text{PAR})z} \tag{3}$$

where $\mathring{E}(\text{PAR}, z_{\text{int}})$ is PAR at the ice-water interface and $K_{\mathring{E}_d}$(PAR) is the diffuse vertical attenuation coefficient (m$^{-1}$) describing the rate at which $\mathring{E}$(PAR) decreases with increasing depth. It is assumed constant for a given station in all our calculations. The determination coefficients ($R^2$) of the nonlinear fits (equation (3)) varied between 0.936 and 0.998.

#### 2.3.2. SUIT Measurements

On the SUIT, transmittance ($T$) and sea ice draft observations were made using a mounted environmental sensors array that included a RAMSES-ACC irradiance sensor (Trios, GmbH, Rastede, Germany), a CTD probe (Sea and Sun Technology, Trappenkamp, Germany), a PA500/6S altimeter (Tritech International Ltd., Aberdeen, UK), and an Aquadopp acoustic DopplerCurrent Profiler (ADCP; Nortek AS, Rud, Norway). A complete and detailed description of the full sensor array can be found in David et al. (2015) and Lange et al. (2016). Sea ice draft was calculated from the CTD depth and altimeter measurements of the distance to the ice and corrected for sensor attitude using the ADCP's pitch and roll measurements according to Lange et al. (2016). Irradiance above the ice was measured with a RAMSES spectroradiometer mounted on the ship's crow's nest. Consistent with the ROV spectral measurements, the transmittance was calculated as the ratio of underice irradiance to incoming irradiance. SUIT-mounted downwelling irradiance measurements were acquired every 11 s during the haul. To account for SUIT movement, all data with SUIT roll and pitch angles larger than 15° were rejected from further analysis. Note that we did not correct for the light attenuation between the ice-water interface and the sensor because contrary to the ROV, the SUIT frame is equipped with buoyancy blocks that keep it at the surface in open water or in contact with the sea ice.

### 2.4. Incident In-Air $\mathring{E}$(PAR)

A CM 11 global radiation pyranometer (Kipp & Zonen, Delft, Netherlands) installed in the crowsnest onboard the Polarstern was used for measuring incident solar photosynthetically available radiation, ($\mathring{E}$(PAR), W/m$^2$), at 10-min intervals. Conversion from shortwave flux in energy units to $\mathring{E}$(PAR) in quanta

($\mu mol \cdot m^{-2} \cdot s^{-1}$) was achieved using a conversion factor of 4.49 (McCree, 1972). Data were then hourly averaged. Calculated hourly $\mathring{E}(\mathrm{PAR}, 0^+)$ were vertically propagated in the water column between 0 and 40 m with 1-m increments using the following equation:

$$\begin{aligned} \mathring{E}(\mathrm{PAR}, z, t) &= \mathring{E}(\mathrm{PAR}, 0^+, t) T(z_{\mathrm{int}}) e^{-K_{\mathring{E}_d}(\mathrm{PAR})z} \\ &= \mathring{E}(\mathrm{PAR}, z_{\mathrm{int}}) e^{-K_{\mathring{E}_d}(\mathrm{PAR})z} \end{aligned} \tag{4}$$

where $\mathring{E}(\mathrm{PAR}, 0^+, t)$ is the incident in-air hourly PAR derived from the pyranometer ($\mu mol \cdot m \cdot s^{-1}$), $K_{\mathring{E}_d}(\mathrm{PAR})$ is derived from the ROV (see Table 1 and equation (3)), $z$ the water depth (m), and $T(z_{\mathrm{int}})$ the snow and sea ice transmittance estimated using either the ROV or the SUIT data.

### 2.5. Photosynthetic Parameters Derived From *P* Versus *E* Curves

To calculate photosynthetic parameters (see the next section for a complete description of these parameters), seawater samples were taken from six depths between 1 and 75 m and incubated at different irradiance levels in presence of $^{14}C$-labeled sodium bicarbonate using a method derived from Lewis and Smith (1983). Incubations were carried out in a dimly lit radiation van under the deck to avoid any light stress on the algae. Three replicates of 50-mL samples were inoculated with inorganic $^{14}C$ ($NaH^{14}CO_3$, ≈2 μCi/ml final concentration). Exact total activity of added bicarbonate was determined by three 20-μL aliquots of inoculated samples added to 50 μL of an organic base (ethanolamine) and 6 ml of scintillation cocktail (EcoLumeTM, Costa Mesa, US) into glass scintillation vials. One millliter aliquots of the inoculated sample were dispensed into twenty-eight 7-ml glass scintillation vials. The samples were cooled to 0 °C in thermoregulated alveoli. Within the array, the vials were exposed to 28 different irradiance levels provided by separate LEDs (LUXEON Rebel, Philips Lumileds, USA) from the bottom of each alveolus. Scalar PAR irradiance was measured in each alveolus prior to the incubation with an irradiance quantum meter (Walz US-SQS + LI-COR LI-250A, USA) equipped with a $4\pi$ spherical collector. For each measurement, the range of irradiance intensities was selected in order to adequately capture the initial slope and maximum part of the *P* versus *E* curve. Because this depends on the in situ growth irradiance, incubation irradiances were modified according to the depth at which the sample was collected. The maximum irradiance varied between 124 and 1,143 μmol photon$\cdot m^{-2} \cdot s^{-1}$. The incubation lasted for 120 min and the incubations were terminated by adding with 50 μL of buffered formalin to each sample. Note that given the short incubation time, our method for deriving primary production likely provides values close to gross production (Lewis & Smith, 1983). Thereafter, the aliquots were acidified (250 μL of HCl 50%) in a glove box (radioactive $^{14}CO_2$ was trapped in a NaOH solution before opening the glove box) to remove the excess inorganic carbon (3 hr, Knap et al., 1996). In the end, 6 ml of scintillation cocktail was added to each vial prior to counting in a liquid scintillation counter (Tri-Carb, PerkinElmer, Boston, USA). The carbon fixation rate was finally estimated according to Parsons et al. (1984). Photosynthetic parameters were estimated from *P* versus *E* curves by fitting nonlinear models based on the original definition proposed by Platt et al. (1980) using equation (5) (parameters are presented in the next section):

$$P(z) = (1 - e^{-\alpha(z)\frac{\mathring{E}(\mathrm{PAR},z)}{z}}) \times e^{-\beta(z)\frac{\mathring{E}(\mathrm{PAR},z)}{z}} + P0 \tag{5}$$

### 2.6. Estimating Primary Production

Two different approaches were used to calculate primary production from estimated photosynthetic parameters.

*Method 1: Underice-only primary production*. This first approach relied on using $\mathring{E}(\mathrm{PAR})$ propagated in the water column only under the ice using the transmittance values derived from either the ROV or the SUIT, the $K_{\mathring{E}_d}(\mathrm{PAR})$ from the ROV, and the hourly incident irradiance from the pyranometer. Primary production was calculated every hour at each sampling depth using $\mathring{E}(\mathrm{PAR}, z, t)$ measurements derived from both ROV and SUIT transmittance as follows:

$$P^{\mathrm{device}}_{\mathrm{underice}}(z, t) = P(z)(1 - e^{-\alpha(z,t)\frac{\mathring{E}(\mathrm{PAR},z,t)}{z}}) \times e^{-\beta(z,t)\frac{\mathring{E}(\mathrm{PAR},z,t)}{z}} \tag{6}$$

where $P^{\mathrm{device}}_{\mathrm{underice}}$ device is primary production ($mgC \cdot m^{-3} \cdot hr^{-1}$) calculated using the $\mathring{E}(\mathrm{PAR}, z, t)$ from the transmittances measured from a specific device (ROV, $P^{\mathrm{ROV}}_{\mathrm{underice}}$ or SUIT, $P^{\mathrm{SUIT}}_{\mathrm{underice}}$), $P$ is the photosynthetic rate ($mgC \cdot m^{-3} \cdot hr^{-1}$) at light saturation, $\alpha$ is the photosynthetic efficiency at irradiance close to zero ($mgC \cdot m^{-3} \cdot hr^{-1}$ (μmol photon$\cdot m^{-2} \cdot s^{-1})^{-1}$), $\beta$ is a photoinhibition parameter (same unit as $\alpha$). The superscript *device* can be either ROV or SUIT. While fits allowed a variable intercept (*P*0), which tended to be

**Table 2**
*Descriptions of the Symbols Used to Identify the Four Types of Primary Production Modeled in This Study*

| Symbol | Description |
|---|---|
| $P_{\text{openwater}}$ | Primary production estimated using 100% transmittance |
| $P^{\text{ROV}}_{\text{underice}}$ | Primary production estimated using underice transmittance values measured by the ROV |
| $P^{\text{ROV}}_{\text{mixing}}$ | Primary production estimated using a miing model approach combining underice transmittance values measured by the ROV and satellite-derived SIC |
| $P^{\text{SUIT}}_{\text{underice}}$ | Primary production estimated using underice transmittance values measured by the SUIT |
| $P^{\text{SUIT}}_{\text{underice}}$ | Primary production estimated using a mixing model approach combining underice transmittance values measured by the SUIT and satellite-derived SIC |

*Note*. ROV = remotely operated vehicle; SUIT = surface and underice trawl; SIC = sea ice concentration.

positive, we did not use $P0$ in the primary production computations as we assumed that it was due to methodological issues (e.g., light absorbed before incubation started). Photosynthetic parameters were linearly interpolated between 0- and 40-m depth by 1-m increment. Daily primary production ($\text{mgC}\cdot\text{m}^{-3}\cdot\text{hr}^{-1}$) at each depth was calculated by integrating $P^{\text{device}}_{\text{underice}}(z, t)$ over a 24-hr period. Depth-integrated primary production ($\text{mgC}\cdot\text{m}^{-2}\cdot\text{day}^{-1}$) was then calculated by integrating daily primary production over the first 40 m of the water column. This depth was chosen because it roughly coincides with the depth of the euphotic zone.

*Method 2: Average production under ice and adjacent open waters.* The second approach consisted of using a mixing model based on SIC derived from satellite imagery to upscale at a larger spatial scale the estimates of primary production derived from the ROV and the SUIT. This approach was motivated by the fact that, even far away from the marginal ice zone, there were often large leads that increased the amount of light available to drifting phytoplankton and may have contributed to underice blooms in the vicinity as observed by Assmy et al. (2017). To account for this additional light source available for phytoplankton, primary production was calculated as follows:

$$P^{\text{device}}_{\text{mixing}} = \text{SIC} \times P^{\text{device}}_{\text{underice}} + (1 - \text{SIC}) \times P_{\text{openwater}} \tag{7}$$

where $P^{\text{device}}_{\text{mixing}}$ is the primary production calculated using the mixing model approach with the transmittance values from a specific device, SIC is the sea ice concentration averaged over an area of ≈350 $\text{km}^2$ (the mean of a 9-pixel square with the station within the center pixel). $P^{\text{device}}_{\text{underice}}$ is the primary production calculated underice using transmittance measurements (equation (6) and Method 1 above), and $P_{\text{openwater}}$ the primary production calculated in open water by using a transmittance of 100%. For the mixing-model-based SUIT-derived primary production, $P^{\text{SUIT}}_{\text{mixing}}$, transmittance observations higher than 10% were discarded to remove measurements made under very thin ice and in open leads to avoid accounting twice for open water. In the end, four types of primary production were considered (two devices × two approaches, Table 2).

### 2.7. Error on Primary Production Estimates

For each of the four scenarios ($P^{\text{SUIT}}_{\text{mixing}}$, $P^{\text{ROV}}_{\text{mixing}}$, $P^{\text{SUIT}}_{\text{underice}}$, and $P^{\text{ROV}}_{\text{underice}}$), the average primary production derived from all the transmittance values was viewed as an adequate description of the average primary production produced by drifting phytoplankton cells for a given area. The relative deviation of each individual primary production estimate to the average primary production over all stations was viewed as the error that one would make when measuring light at a single location. This relative error was calculated as follows:

$$\delta^{\text{device}}_{P} = \frac{|P^{\text{device}} - \bar{P}^{\text{device}}|}{\bar{P}^{\text{device}}} \times 100 \tag{8}$$

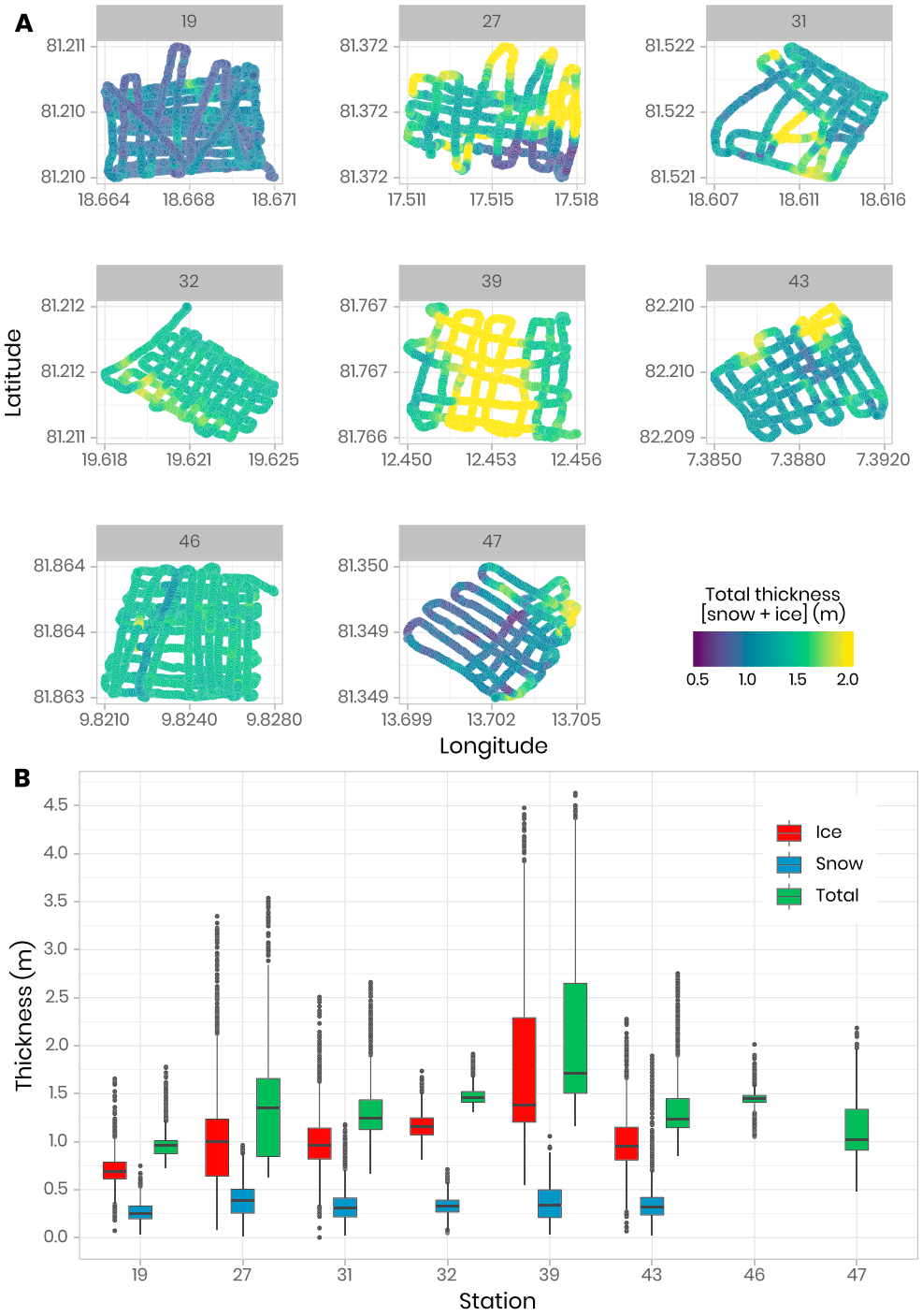


**Figure 2.** (a) Spatial overview of the total thickness (snow + ice) at each station. (b) Boxplots showing the variability and the contribution of the snow and the ice to the total thickness. Note that only total thickness is available at stations 46 and 47 due to instrument failure.

where $\delta_P^{\text{device}}$ is the relative error (%) associated to a specific device (ROV or SUIT), $P^{\text{device}}$ the primary production estimate, and $\bar{P}^{\text{device}}$ the average primary production of the device (both in mgC·m$^{-2}$·day$^{-1}$).

### 2.8. Impacts of the Number of In Situ Single-Location Light Measurements on Primary Production Estimates

Because of the sea surface heterogeneity in the field, one needs to carefully choose the number of single-location light measurements in order to obtain representative values of primary production over a

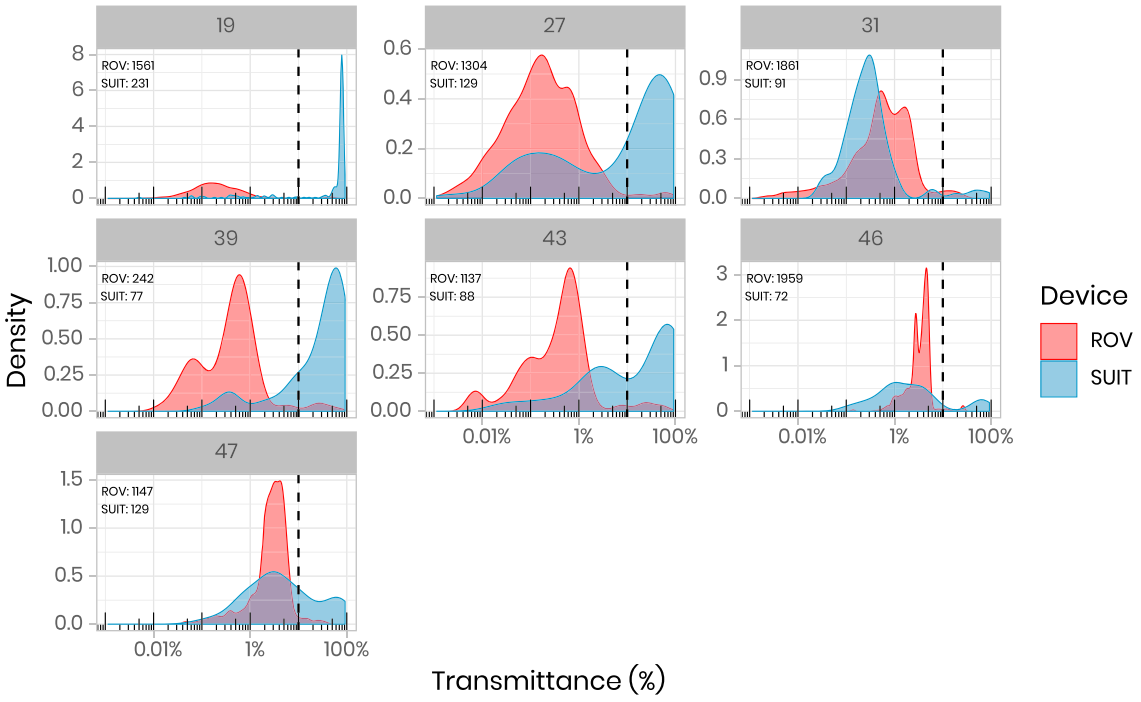


**Figure 3.** Density plots showing the distribution of transmittance values measured by the ROV and the SUIT devices. Dashed lines represent the 10% transmittance threshold used to filter out SUIT transmittance used in the mixing models. Numbers on top of the gray boxes identify the stations. Top-left numbers in each facet show the number of observations. ROV = remotely operated vehicle; SUIT = surface and underice trawl.

given area. Averaging a high number of local measurements is likely to give a better approximation of the average primary production over a given area. However, in the Arctic, it is difficult to sample a high number of uniformly dispersed sampling locations due to logistical constraints. Using primary production estimates derived from the ROV and the SUIT, we calculated how the error would decrease on average when increasing the number of measurements uniformly sampled over a given area. To calculate this error, between 1 and 250 values were randomly drawn from the full distribution of primary production values calculated with individual transmittance data from the ROV or SUIT and used to calculate average primary production. One can view each of these 250 numerical experiments as possible number of single-location irradiance measurements that one would perform in the field. Each numerical experiment was repeated 100 times to calculate an average and the standard deviation of the absolute difference between a given estimate of primary production and the reference primary production calculated with all transmittance measurements.

### 2.9. Statistical Analysis

All statistical analysis and graphics were carried out with R 3.6.0 (R Core Team, 2019). The nonlinear fitting for the $P$ versus $E$ curves was done using the Levenberg-Marquardt algorithm implemented in the minpack.lm R package (Elzhov et al., 2013). The code used in this study is available under the GNU GPLv3 license (https://github.com/PMassicotte/transsiz).

## 3. Results

### 3.1. Characterization of the Sea Ice and Snow Cover

GEM-2 and Magna Probe surveys along and across the ROV transects showed distinct differences in sea ice and snow thickness between the sampled stations. An overview of the total thickness (i.e., combined snow and ice thickness) is presented in Figure 2a. Overall, the mean ice thickness was 1.01 ± 0.52 m (mean ± s.d.), the mean snow thickness was 0.32 ± 0.16 m and the mean total thickness was 1.33 ± 0.49 m (Figure 2b). Stations 19 and 47 were characterized by an average total thickness over the ROV transect of ≈1 m, whereas the average total thickness at station 39 was ≈2 m. For other stations, average total thickness varied around 1.4 m.

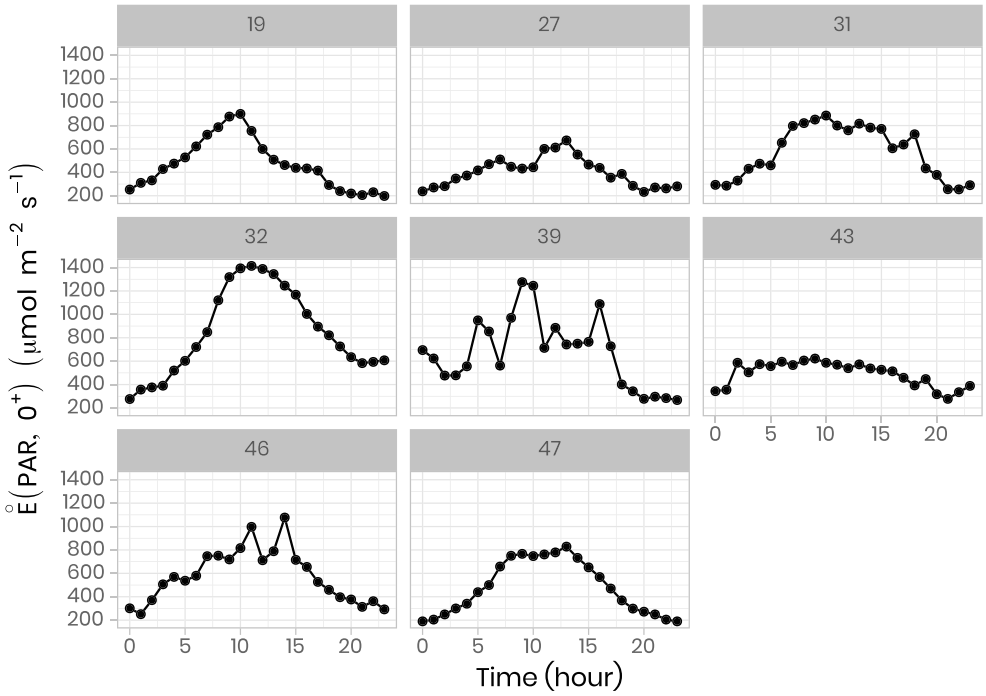


**Figure 4.** Incident hourly photosynthetic active radiation, $\mathring{E}(\mathrm{PAR}, 0^+, t)$, measured at each station with a pyranometer installed onboard the ship. Numbers on top of the gray boxes identify the stations.

### 3.2. ROV and SUIT Transmittance Measurements

A total of 9,211 and 817 transmittance measurements distributed over the seven stations were collected from the ROV and SUIT devices, respectively (Figure 3). Transmittance values ranged between 0.001% and 68% for the ROV and between 0.002% and 92% for the SUIT (Figure 3). The transmittances measured by the SUIT were generally higher (mean = 35%) by ≈1 order of magnitude than those measured with the ROV (mean = 2%). The SUIT measurements were also covering greater ranges of transmittances compared to the ROV. Histograms showed that transmittance generally followed a bimodal distribution (most of the time occurring within the SUIT data) with often one overlapping mode between the ROV and SUIT values (Figure 3).

### 3.3. PAR

Incident hourly $\mathring{E}(\mathrm{PAR})$, $\mathring{E}(\mathrm{PAR}, 0^+, t)$, measured by the pyranometer ranged between 190 and 1,400 µmol·m$^{-2}$·s$^{-1}$ (Figure 4). Stations 32 and 39 experienced the highest incident $\mathring{E}(\mathrm{PAR}, 0^+, t)$ whereas stations 27 and 43 received the lowest amount of light. Over 24-hr periods, $\mathring{E}(\mathrm{PAR}, z_{\mathrm{int}})$ calculated using SUIT and ROV transmittances ranged between 0.005–1,358 and 0.005–1,012 µmol·m$^{-2}$·s$^{-1}$, respectively. Due to relatively high attenuation coefficients (Table 1), $\mathring{E}(\mathrm{PAR})$ decreased rapidly with depth and generally reached the asymptotic regime at maximum 30-m depth. The PAR diffuse vertical attenuation coefficients, $K_{\mathring{E}_d}(\mathrm{PAR})$, estimated from the ROV vertical profiles varied between 0.07 and 0.59 m$^{-1}$ (Table 1).

### 3.4. Estimated Primary Production

Daily areal primary production derived from photosynthetic parameters and transmittance values ranged between 0.004 and 939 mgC·m$^{-2}$·day$^{-1}$ for $P_{\mathrm{underice}}$ and between 0.004 and 731 mgC·m$^{-2}$·day$^{-1}$ for $P_{\mathrm{mixing}}$ (Figure 5). In ROV-based estimates, daily areal primary production calculated using the two different approaches ($P_{\mathrm{underice}}$ and $P_{\mathrm{mixing}}$) generally showed consistency especially when SIC was high. At stations 19 and 27, greater differences between $P_{\mathrm{underice}}$ and $P_{\mathrm{mixing}}$ were observed in ROV-based estimates due to lower sea ice concentrations (Table 1) which allowed for a greater weight of $P_{\mathrm{openwater}}$ on the calculations. In SUIT-based estimates, mean daily $P_{\mathrm{underice}}$ values were higher than $P_{\mathrm{mixing}}$ values at stations 19, 39, and 43, similar at stations 27, 46, and 47, and lower at station 31 (Figure 5). The 10% transmittance threshold used to filter out SUIT-based data explains why mean values of daily $P_{\mathrm{underice}}$ can be lower than those based on ROV measurements. The differences between the two approaches in SUIT data were related to the varying proportions of thin ice and open water during SUIT hauls, which were reflected in the $P_{\mathrm{underice}}$ estimates. Overall,

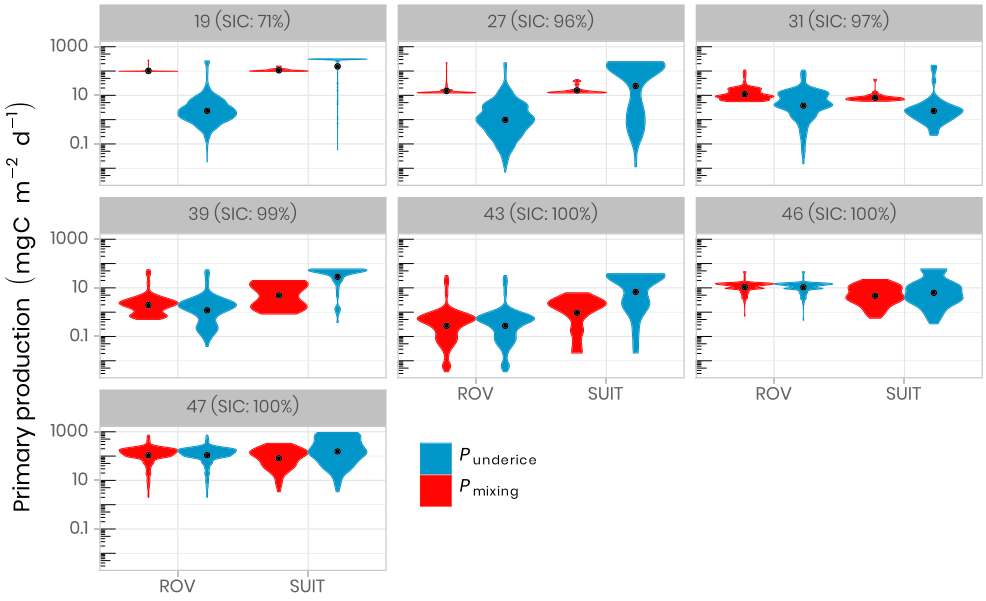


**Figure 5.** Violin plots of primary production calculated from ROV and SUIT transmittance data. For SUIT data, mixing models were calculated using only transmittance ≤10% (see Figure 3), whereas the under ice models were calculated using all transmittance data. Black dots inside the violin plots indicate the average primary production. Numbers on top of the gray boxes identify the stations and satellite-derived sea ice concentrations. SIC = sea ice concentration; ROV = remotely operated vehicle; SUIT = surface and underice trawl.

both ROV- and SUIT-based estimates agreed well with each other when the mixing approach ($P_{mixing}$) was applied.

### 3.5. Error On Primary Production Estimates

Figure 6 shows the distributions of the relative errors around the calculated average of areal primary production (see black dots in Figure 5). Overall, the absolute relative errors ($\delta_P$) were distributed over a range covering 4 orders of magnitude, between 0.1% and 1000%, which corresponds to an absolute pri-

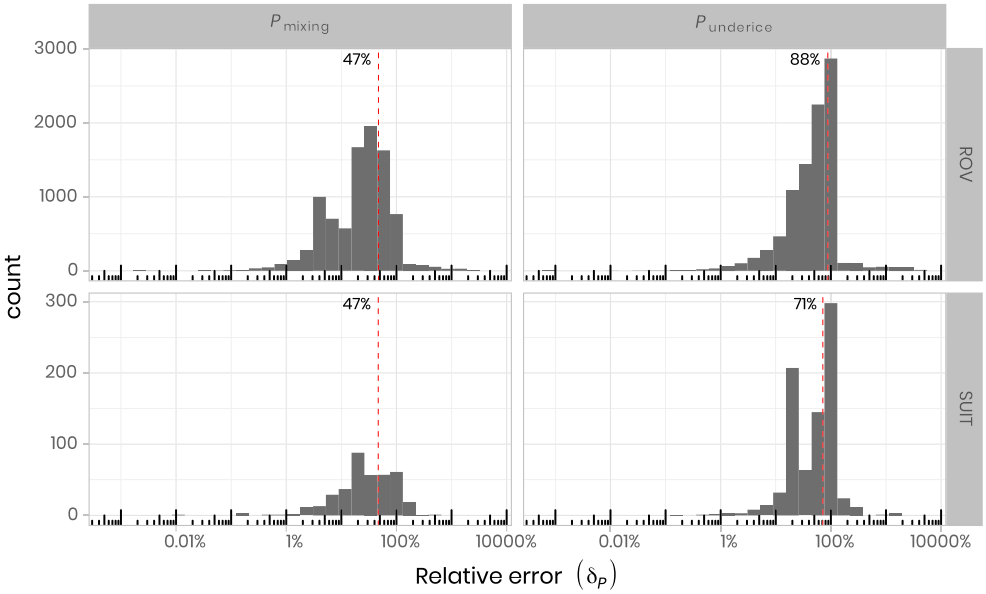


**Figure 6.** Distributions of the relative errors corresponding to the absolute deviation of each individual primary estimations from the average (see equation (7) for details). The red dashed lines and the numbers on the left indicate the mean errors. ROV = remotely operated vehicle; SUIT = surface and under-ice trawl.

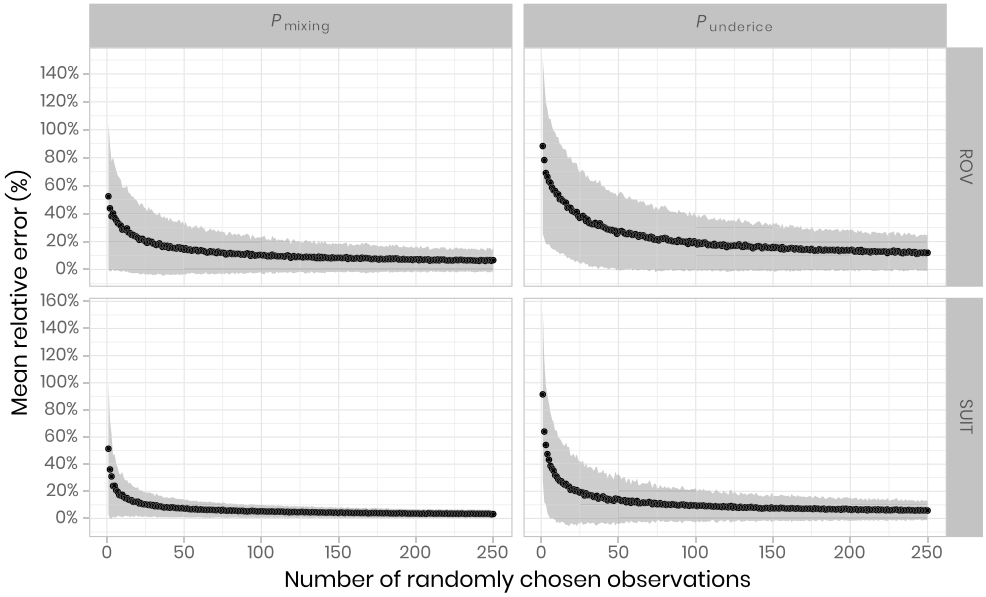


**Figure 7.** Average relative errors based on the number of single-spot measurements that one would make when averaging samples randomly sampled over a given area (black dots). The shaded gray areas represent the standard deviation around the mean. The means and standard deviations were calculated from 100 randomly chosen replicates. ROV = remotely operated vehicle; SUIT = surface and under-ice trawl.

mary production error varying between 0.0001 and 640 mgC·m$^{-2}$·day$^{-1}$. The lowest absolute errors (average ≈50%) were associated with primary production estimates made using the mixing model approach ($P_{mixing}$). Larger absolute errors were made with $P_{underice}$ derived from only using ROV (mean = 88%) and the SUIT (mean = 71%) transmittances.

### 3.6. Impacts of the Number of In Situ Light Measurements on Primary Production Estimates

Figure 7 shows the average relative error that one would make when averaging light measurements performed at a number of random locations varying between 1 and 250. The variability around the means also decreased with increasing number of observations (shaded areas in Figure 7). The greatest relative mean error (≈60–100%) occurred when only one primary production estimate was randomly selected from the distributions. The number of randomly selected observations to reach mean relative errors of 10%, 15%, 20%, and 25% are presented in Table 3. Overall, about 25% of the number of observations were needed to reach those targets when sampling from the distribution for $P_{mixing}$ compared to the distribution of $P_{underice}$. Additionally, the number of observations required when using the SUIT transmittance to derive primary production estimation was also about 25% of the number of corresponding ROV-based measurements to reach the same error threshold.

## 4. Discussion

### 4.1. Primary Production Under Heterogeneous Sea Ice

Vertically integrated net primary production in the Arctic is known to be highly variable in both time and space (Hill et al., 2018; Matrai et al., 2013). For example, primary production in the central Arctic

**Table 3**
*Number of Measurements Needed to Reach Various Relative Error Thresholds*

| Model | Relative error threshold | | | |
|---|---|---|---|---|
| | 10% | 15% | 20% | 25% |
| $PP^{ROV}_{mixing}$ | 99 | 46 | 26 | 16 |
| $PP^{ROV}_{underice}$ | 359 | 166 | 90 | 60 |
| $PP^{SUIT}_{mixing}$ | 27 | 13 | 7 | 5 |
| $PP^{SUIT}_{underice}$ | 86 | 40 | 23 | 15 |

Ocean estimated using photosynthetic parameters was found to vary between 18 and 308 mgC·m$^{-2}$·day$^{-1}$ in ice-free waters, and between 0.1 and 232 mgC·m$^{-2}$·day$^{-1}$ in ice-covered waters (Fernández-Méndez et al., 2015). Our primary production estimates generally fall within these ranges, although our highest values (731–939 mgC·m$^{-2}$·day$^{-1}$) are roughly twice as high. There are many factors such as season, cloudiness, sea ice and snow, nutrient concentration, temperature, and phytoplankton community composition that can influence such variability. In a modeling exercise, Popova et al. (2010) found that shortwave light radiation and the maximum depth of winter mixing (which determine the amount of nutrients available for summer primary production) explained more than 80% of the spatial variability of primary production in the Arctic. In our approach, the impact of light history, nutrients, temperature, and community composition are implicit in photosynthetic parameters and chl *a* concentration obtained in this study. The instantaneous effect of light variations is explicit and the main focus of this study.

### 4.2. Multiscale Spatial Variability of Light Transmittance

In the context of obtaining meaningful measurements of transmittance to accurately estimate $\mathring{E}$(PAR, 0-), one challenge is to define the spatial extent at which light should be sampled. Based on a spatial autocorrelation analysis conducted in the central Arctic Ocean, it was determined that transmittance values were uncorrelated (i.e., randomly spatially distributed) to each other after a horizontal lag distance of 65 m (Lange et al., 2017). This range is much smaller than the distance covered by drifting phytoplankton over a 24-hr period. Water currents around Svalbard have been found to vary between 0.14 and 0.21 m/s at this time of the year (Meyer et al., 2017). Such speeds are in the same order of magnitude as the average sea ice drift speeds of 0.10 m/s observed during the expedition. On daily time scales, ice motion is generally decoupled from ocean currents and is rather driven by inertial oscillations and wind stress (Park & Stewart, 2016). This corresponds to a relative ice-water displacement varying between 3.5 and 18 km over a 24-hr period, which is much greater than the scale of the spatial variability of transmittance, as well as the scale of most typical ice floes in this area. Under such a large area, drifting phytoplankton is experiencing a wide range of irradiance conditions that can be hardly characterized by a single-location light measurement. Our results showed that at medium spatial scales, the ROV and the SUIT are able to characterize the local sea ice variability on the scale of one or a few individual ice floes. However, these technologies do not adequately capture the spatial variability that originates from larger-scale features such as open water areas nor large leads that can increase the amount of light available to drifting phytoplankton (Assmy et al., 2017). Thus, at larger spatial scales, satellite-derived information, such as SIC or lead cover products can provide important information on the panarctic context. Such information allows to upscale the estimates of primary production derived from the ROV and the SUIT to a larger spatial scale. Our results showed that using a simple mixing model (equation (7)), combining both in situ transmittance measurements and SIC, can be used to upscale observations acquired "locally" to larger scales. This approach reduced the relative error by approximately a factor of 2 when spatially integrating devices such as ROVs or SUIT are used to measure transmittance (Figure 5). Furthermore, this error was lower when using in situ measurements acquired on a larger spatial scale using the SUIT. This strengthens the idea that one needs to characterize the light field over an area as large as reasonably possible so the true irradiance variability is captured.

Our study confirms our earlier hypothesis that estimating primary production from photosynthetic parameters and transmittance measured at a single location does not provide a representative description of the spatial variability of the primary production occurring under a heterogeneous sea surface (Figures 6 and 7). Depending on the scale at which transmittance was measured, it was found that deriving primary production from photosynthetic parameters using underice profile measurements alone would produce on average relative errors varying between 47% and 88% (Figure 6). In contrast, much lower errors (25%) were made when primary production estimates were upscaled using satellite-derived SIC ($P_{\mathrm{mixing}}$). For stations with lower SIC (stations 19, 27, 31, and 39), primary production estimates were more constrained around the average (Figure 4) because $P_{\mathrm{openwater}}$ had a greater weight in the calculation of $P_{\mathrm{mixing}}$ (see equation (7)). For stations 43, 46, and 47 where SIC was 100%, the spread around the mean was higher because only $P_{\mathrm{underice}}$ was contributing to the calculation of $P_{\mathrm{mixing}}$. These results suggest that using a distribution of measured transmittances allows calculating a more representative transmittance average for a given area but also provides additional knowledge on its spatial variability.

Although our results indicate that it is necessary to properly characterize the light field under the heterogeneous sea surface, the physiological state of the phytoplankton community under the sea ice surface also plays a major role on the sensitivity of the estimates to incoming irradiance. An important parameter of

the physiological state of the phytoplankton community is the light-saturated photosynthesis regime, $E_k$ an index of photoadaptation. If a phytoplankton community was adapted to extremely low light intensity, as example, variations in the surface light field would have reduced impacts on the estimates because phytoplankton primary production might be systematically light saturated. In this study, the average $E_k$ was 65.2 ± 55.3 (range = 18.0–409.5) μmol·m$^{-2}$·s$^{-1}$, whereas the average of all estimates of mean daily, underice irradiance made from ROV and SUIT measurements was 12.6 ± 7.6 (range = 3.0–26.4) μmol·m$^{-2}$·s$^{-1}$. Since the latter were generally much lower than $E_k$, phytoplankton were able to respond strongly to variability in the underice light field and take advantage of increased irradiance in occasional leads. This setting underscores the importance of taking into account a mixture of sea ice cover and open water, for the estimation of primary production. However, the seasonal degree of photoadaptation of the phytoplankton communities and their ability to adjust rapidly to a variable light field still remains to be evaluated.

### 4.3. Influence of the Number of Sampling Locations on Primary Production Estimation

As with any scientific expedition in remote environments such as the Arctic, careful planning is needed to find the right balance between the sampling effort and the sufficient amount of acquired information to study a particular phenomenon. Our results suggested that errors made by estimating primary production using photosynthetic parameters decreased exponentially with increasing number of transmittance measurements (Figure 7). Depending on the extent of the spatial scale at which transmittance is measured (order of meters for the ROV, order of kilometers for the SUIT) and the targeted error thresholds (10%, 15%, 20% or 25%), a number of light measurements varying between four and 359 were sufficient to reasonably capture the spatial variability of sea ice transmittance to derive average primary production estimates over a given area. This shows that local primary production estimated from just a single or even a handful of light observations has limited value. However, further seasonal and regional studies are needed to fully capture the variability of photosynthetic parameters, which are not fully accounted for within the primary production derived from the presented spring study.

### 4.4. Implications for Arctic Primary Production Estimates

It is known that the annual primary production in the ice-covered Arctic is among the lowest of all oceans worldwide, because both light and limited nutrient availability are the main constraining factors for phytoplankton growth under the ice. In a changing Arctic icescape, efforts have been devoted to better understand how phytoplankton primary production is responding to increasing light availability (Fernández-Méndez et al., 2015; Vancoppenolle et al., 2013). Many studies have been conducted in the vicinity of an ice edge to characterize primary production occurring under the ice sheet (Arrigo et al., 2012, 2014; Mundy et al., 2009). However, in such studies, due to logistical constraints, the underwater light field was often characterized by a limited number of light measurements. Other approaches, based on 24-hr ship-board incubations performed under incident light, have provided local estimates that were simply scaled to an assessment of percent ice cover in the vicinity of the ship (Gosselin et al., 1997; Mei et al., 2003; Smith, 1995). Therefore, depending on whether light is measured under bare ice or in open water, the estimated primary production is either underestimated or overestimated. Different approaches based on remote sensing techniques and modeling have been used to reduce the uncertainties associated with estimates derived from local in situ measurements. However, in an ecosystem model intercomparison study, Jin et al. (2016) showed that underice primary production was very sensitive to the light availability computed by atmospheric and sea ice models, reinforcing the need to develop new integrative strategies to adequately characterize the light field at large scale under heterogeneous sea ice surfaces. Our results show that upscaling primary production estimates derived from fine-scale local measurements using SIC derived from satellite imagery allowed reducing the error at larger spatial scales. Furthermore, it was found that even when SIC was high (>95%), the use of a mixing-model approach helped to obtain better estimates (Figure 5).

Based on our results, different strategies can be easily adopted to obtain the best possible estimates of primary production under spatially heterogeneous sea ice surfaces. First, one should acquire a sufficient number of $P$ versus $E$ curves under different nutrient conditions that are representative for the region under investigation. Second, one should measure light transmittance or irradiance at a spatial scale fine enough to capture the horizontal variability that is meaningful for the studied process. The number of measurements should be chosen as a function of the sampling method and a reasonable degree of error (Figure 7 and Table 3). Nowadays, this can be relatively easily achieved using ROV, SUIT, or autonomous underwater vehicles. Third, under heterogeneous sea ice surface, one should use extinction coefficients derived from upward radiance ($L_u$) measurements to propagate PAR in the water column because it is less influenced by the geometric

effects of sea ice surface compared to downward irradiance (Katlein et al., 2016; Massicotte et al., 2018). Finally, local measurements can be upscaled at higher spatial scale using remote sensing data such as sea ice concentration.

## 5. Conclusions

Advances in underwater technologies have made it easier to characterize surface transmittance over large areas even under dense sea ice. Our results show that combining photosynthetic parameters measured in laboratory experiments with spatially representative transmittance values sampled with underice profiling platforms can significantly improve the accuracy of primary production estimates under heterogeneous sea surfaces. A good way forward to sample the underice light field on a large enough scale without the inherent biases of the ROV and SUIT deployment techniques would be the use of long-range autonomous underwater vehicles. Furthermore, upscaling in situ measurements at larger scales using remote sensing data becomes necessary when the spatial scale of the studied process (e.g., a phytoplankton bloom) is greater than that which is realistically possible to measure in the field. This emphasizes the need for spatially integrated observation approaches to characterize the light field in ice-covered regions in order to provide more representative primary production estimates for the Arctic.

**Acknowledgments**
We thank F. Bruyant and M. Beaulieu for carrying out the *P* versus *E* curve measurements and providing us with the data. We thank Sascha Willmes for onboard processing of the ice and snow thickness data. We thank Captain Thomas Wunderlich and the crew of icebreaker Polarstern for their support during the TRANSSIZ campaign (AWI_PS92_00). This study was conducted under the Helmholtz Association Research Programme Polar regions And Coasts in the changing Earth System II (PACES II), Topic 1, WP 4 and is part of the Helmholtz Association Young Investigators Groups Iceflux: Ice-ecosystem carbon flux in polar oceans (VH-NG-800). B. A. L. was partly funded during this study by a Visiting Fellowship from the Natural Sciences and Engineering Research Council of Canada (NSERC). The project was conducted under the scientific coordination of the Canada Excellence Research Chair on Remote sensing of Canada's new Arctic frontier and the CNRS and Université Laval Takuvik Joint International laboratory (UMI3376). We also acknowledge the Sentinel North Strategy for their financial support. SUIT was developed by Wageningen Marine Research (WMR; formerly IMARES) with support from the Netherlands Ministry of EZ (project WOT-04-009-036) and the Netherlands Polar Program (project ALW 866.13.009). We thank Jan Andries van Franeker (WMR) for kindly providing the Surface and Under Ice Trawl (SUIT) and Michiel van Dorssen for technical support with work at sea. Data for the light measurement used in this study can be found on Pangaea website. ROV data (https://doi.pangaea.de/10.1594/PANGAEA.861048), incident radiation (https://doi.pangaea.de/10.1594/PANGAEA.849663), station list (https://doi.pangaea.de/10.1594/PANGAEA.848841), SUIT data (https://doi.pangaea.de/10.1594/PANGAEA.902056), photosynthetic parameters (https://doi.org/10.1594/PANGAEA.899842), and sea-ice/snow thickness (https://doi.pangaea.de/10.1594/PANGAEA.897958).

## References

Ambrose, W. G., von Quillfeldt, C., Clough, L. M., Tilney, P. V. R., & Tucker, T. (2005). The sub-ice algal community in the Chukchi sea: Large- and small-scale patterns of abundance based on images from a remotely operated vehicle. *Polar Biology*, *28*(10), 784–795. https://doi.org/10.1007/s00300-005-0002-8

Arrigo, K. R., Perovich, D. K., Pickart, R. S., Brown, Z. W., van Dijken, G. L., Lowry, K. E., et al. (2012). Massive phytoplankton blooms under Arctic sea ice. *Science*, *336*(6087), 1408–1408. https://doi.org/10.1126/science.1215065

Arrigo, K. R., Perovich, D. K., Pickart, R. S., Brown, Z. W., van Dijken, G. L., Lowry, K. E., et al. (2014). Phytoplankton blooms beneath the sea ice in the Chukchi Sea. *Deep Sea Research Part II: Topical Studies in Oceanography*, *105*, 1–16. https://doi.org/10.1016/j.dsr2.2014.03.018

Assmy, P., Fernández-Méndez, M., Duarte, P., Meyer, A., Randelhoff, A., Mundy, C. J., et al. (2017). Leads in Arctic pack ice enable early phytoplankton blooms below snow-covered sea ice. *Scientific Reports*, *7*(1), 40850. https://doi.org/10.1038/srep40850

David, C., Lange, B., Rabe, B., & Flores, H. (2015). Community structure of under-ice fauna in the Eurasian central Arctic Ocean in relation to environmental properties of sea-ice habitats. *Marine Ecology Progress Series*, *522*, 15–32. https://doi.org/10.3354/meps11156

Elzhov, T. V., Mullen, K. M., Spiess, A.-N., & Bolker, B. (2013). minpack.lm: R interface to the Levenberg-Marquardt nonlinear least-squares algorithm found in MINPACK, plus support for bounds. http://cran.r-project.org/package=minpack.lm

Fernández-Méndez, M., Katlein, C., Rabe, B., Nicolaus, M., Peeken, I., Bakker, K., et al. (2015). Photosynthetic production in the central Arctic Ocean during the record sea-ice minimum in 2012. *Biogeosciences*, *12*(11), 3525–3549. https://doi.org/10.5194/bg-12-3525-2015

Flores, H., van Franeker, J. A., Siegel, V., Haraldsson, M., Strass, V., Meesters, E. H., et al. (2012). The Association of Antarctic Krill Euphausia superba with the under-ice habitat. *PLoS One*, *7*(2), e31775. https://doi.org/10.1371/journal.pone.0031775

Frey, K. E., Perovich, D. K., & Light, B. (2011). The spatial distribution of solar radiation under a melting Arctic sea ice cover. *Geophysical Research Letters*, *38*, L22501. https://doi.org/10.1029/2011GL049421

Gosselin, M., Levasseur, M., Wheeler, P. A., Horner, R. A., & Booth, B. C. (1997). New measurements of phytoplankton and ice algal production in the Arctic Ocean. *Deep-Sea Research Part II: Topical Studies in Oceanography*, *44*(8), 1623–1644. https://doi.org/10.1016/S0967-0645(97)00054-4

Hancke, K., Lund-Hansen, L. C., Lamare, M. L., Højlund Pedersen, S., King, M. D., Andersen, P., & Sorrell, B. K. (2018). Extreme low light requirement for algae growth underneath sea ice: A Case Study From Station Nord, NE Greenland. *Journal of Geophysical Research: Oceans*, *123*, 985–1000. https://doi.org/10.1002/2017JC013263

Hill, V., Ardyna, M., Lee, S. H., & Varela, D. E. (2018). Decadal trends in phytoplankton production in the Pacific Arctic Region from 1950 to 2012. *Deep-Sea Research Part II: Topical Studies in Oceanography*, *152*, 82–94. https://doi.org/10.1016/j.dsr2.2016.12.015

Itkin, P., Spreen, G., Cheng, B., Doble, M., Girard-Ardhuin, F., Haapala, J., et al. (2017). Thin ice and storms: Sea ice deformation from buoy arrays deployed during N-ICE2015. *Journal of Geophysical Research: Oceans*, *122*, 4661–4674. https://doi.org/10.1002/2016JC012403

Jin, M., Popova, E. E., Zhang, J., Ji, R., Pendleton, D., Varpe, Ø., et al. (2016). Ecosystem model intercomparison of under-ice and total primary production in the Arctic Ocean. *Journal of Geophysical Research: Oceans*, *121*, 934–948. https://doi.org/10.1002/2015JC011183

Katlein, C., Arndt, S., Nicolaus, M., Perovich, D. K., Jakuba, M. V., Suman, S., et al. (2015). Influence of ice thickness and surface properties on light transmission through Arctic sea ice. *Journal of Geophysical Research: Oceans*, *120*, 5932–5944. https://doi.org/10.1002/2015JC010914

Katlein, C., Perovich, D. K., & Nicolaus, M. (2016). Geometric Effects of an inhomogeneous sea ice cover on the under ice light field. *Frontiers in Earth Science*, *4*(6). https://doi.org/10.3389/feart.2016.00006

Katlein, C., Schiller, M., Belter, H. J., Coppolaro, V., Wenslandt, D., & Nicolaus, M. (2017). A new remotely operated sensor platform for interdisciplinary observations under sea ice. *Frontiers in Marine Science*, *4*, 281. https://doi.org/10.3389/fmars.2017.00281

Knap, A. H., Michaels, A., Close, A. R., Ducklow, H., & Dickson, A. G. (1996). Protocols for the joint global ocean flux study (JGOFS) core measurements.

Kwok, R., Spreen, G., & Pang, S. (2013). Arctic sea ice circulation and drift speed: Decadal trends and ocean currents. *Journal of Geophysical Research: Oceans*, *118*, 2408–2425. https://doi.org/10.1002/jgrc.20191

Lange, B. A., Flores, H., Michel, C., Beckers, J. F., Bublitz, A., Casey, J. A., et al. (2017). Pan-Arctic sea ice-algal chl a biomass and suitable habitat are largely underestimated for multiyear ice. *Global Change Biology*, *23*(11), 4581–4597. https://doi.org/10.1111/gcb.13742

Lange, B. A., Katlein, C., Castellani, G., Fernández-Méndez, M., Nicolaus, M., Peeken, I., & Flores, H. (2017). Characterizing Spatial Variability of ice algal chlorophyll a and net primary production between sea ice habitats using horizontal profiling platforms. *Frontiers in Marine Science*, *4*(November), 1–23. https://doi.org/10.3389/fmars.2017.00349

Lange, B. A., Katlein, C., Nicolaus, M., Peeken, I., & Flores, H. (2016). Sea ice algae chlorophyll a concentrations derived from under-ice spectral radiation profiling platforms. *Journal of Geophysical Research: Oceans*, *121*, 8511–8534. https://doi.org/10.1002/2016JC011991

Lewis, M., & Smith, J. (1983). A small volume, short-incubation-time method for measurement of photosynthesis as a function of incident irradiance. *Marine Ecology Progress Series*, *13*, 99–102. https://doi.org/10.3354/meps013099

Lund-Hansen, L. C., Juul, T., Eskildsen, T. D., Hawes, I., Sorrell, B., Melvad, C., & Hancke, K. (2018). A low-cost remotely operated vehicle (ROV) with an optical positioning system for under-ice measurements and sampling. *Cold Regions Science and Technology*, *151*, 148–155. https://doi.org/10.1016/j.coldregions.2018.03.017

Massicotte, P., Bécu, G., Lambert-Girard, S., Leymarie, E., & Babin, M. (2018). Estimating underwater light regime under spatially heterogeneous sea ice in the Arctic. *Applied Sciences*, *8*(12), 2693. https://doi.org/10.3390/app8122693

Matrai, P. A., Olson, E., Suttles, S., Hill, V., Codispoti, L. A., Light, B., & Steele, M. (2013). Synthesis of primary production in the Arctic Ocean: I. Surface waters, 1954–2007. *Progress in Oceanography*, *110*, 93–106. https://doi.org/10.1016/j.pocean.2012.11.004

McCree, K. J. (1972). Test of current definitions of photosynthetically active radiation against leaf photosynthesis data. *Agricultural and Forest Meteorology*, *10*(C), 443–453. https://doi.org/10.1016/0002-1571(72)90045-3

Mei, Z., Legendre, L., Gratton, Y., Tremblay, J., LeBlanc, B., Klein, B., & Gosselin, M. (2003). Phytoplankton production in the North Water Polynya: Size-fractions and carbon fluxes, April to July 1998. *Marine Ecology Progress Series*, *256*, 13–27. https://doi.org/10.3354/meps256013

Meier, W. N., Hovelsrud, G. K., van Oort, B. E. H., Key, J. R., Kovacs, K. M., Michel, C., et al. (2014). Arctic sea ice in transformation: A review of recent observed changes and impacts on biology and human activity. *Reviews of Geophysics*, *52*, 185–217. https://doi.org/10.1002/2013RG000431

Meyer, A., Sundfjord, A., Fer, I., Provost, C., Villacieros Robineau, N., Koenig, Z., et al. (2017). Winter to summer oceanographic observations in the Arctic Ocean north of Svalbard. *Journal of Geophysical Research: Oceans*, *122*, 6218–6237. https://doi.org/10.1002/2016JC012391

Mundy, C. J., Gosselin, M., Ehn, J., Gratton, Y., Rossnagel, A., Barber, D. G., et al. (2009). Contribution of under-ice primary production to an ice-edge upwelling phytoplankton bloom in the Canadian Beaufort Sea. *Geophysical Research Letters*, *36*, L17601. https://doi.org/10.1029/2009GL038837

Nicolaus, M., Hudson, S. R., Gerland, S., & Munderloh, K. (2010). A modern concept for autonomous and continuous measurements of spectral albedo and transmittance of sea ice. *Cold Regions Science and Technology*, *62*(1), 14–28. https://doi.org/10.1016/j.coldregions.2010.03.001

Nicolaus, M., & Katlein, C. (2013). Mapping radiation transfer through sea ice using a remotely operated vehicle (ROV). *The Cryosphere*, *7*(3), 763–777. https://doi.org/10.5194/tc-7-763-2013

Nicolaus, M., Petrich, C., Hudson, S. R., & Granskog, M. A. (2013). Variability of light transmission through Arctic land-fast sea ice during spring. *The Cryosphere*, *7*(3), 977–986. https://doi.org/10.5194/tc-7-977-2013

Park, H.-S., & Stewart, A. L. (2016). An analytical model for wind-driven Arctic summer sea ice drift. *The Cryosphere*, *10*(1), 227–244. https://doi.org/10.5194/tc-10-227-2016

Parsons, T. R., Maita, Y., & Lalli, C. M. (1984). *A manual of chemical and biological methods for seawater analysis* (1st ed.). Oxford [Oxfordshire]; New York: Pergamon Press.

Perovich, D. K., Roesler, C. S., & Pegau, W. S. (1998). Variability in Arctic sea ice optical properties. *Journal of Geophysical Research*, *103*(C1), 1193–1208. https://doi.org/10.1029/97JC01614

Platt, T., Gallegos, C. L., & Harrison, W. G. (1980). Photoinhibition of photosynthesis in natural assemblages of marine phytoplankton. *Journal of Marine Research*, *38*, 687–701.

Popova, E. E., Yool, A., Coward, A. C., Aksenov, Y. K., Alderson, S. G., Cuevas, B. A. D., & Anderson, T. R. (2010). Control of primary production in the Arctic by nutrients and light: Insights from a high resolution ocean general circulation model. *Biogeosciences*, *7*, 3569–3591. https://doi.org/10.5194/bg-7-3569-2010

R Core Team (2019). R: A language and environment for statistical computing, Vienna, Austria. https://www.r-project.org/

Smith, W. O. (1995). Primary productivity and new production in the Northeast Water (Greenland) Polynya during summer 1992. *Journal of Geophysical Research*, *100*(C3), 4357. https://doi.org/10.1029/94JC02764

Spreen, G., Kaleschke, L., & Heygster, G. (2008). Sea ice remote sensing using AMSR-E 89-GHz channels. *Journal of Geophysical Research*, *113*, C02S03. https://doi.org/10.1029/2005JC003384

Sturm, M., Maslanik, J. A., Perovich, D. K., Stroeve, J. C., Richter-Menge, J., Markus, T., et al. (2006). Snow depth and ice thickness measurements from the Beaufort and Chukchi Seas collected during the AMSR-Ice03 Campaign. *IEEE Transactions on Geoscience and Remote Sensing*, *44*, 3009–3020. https://doi.org/10.1109/TGRS.2006.878236

Toole, D. A., Kieber, D. J., Kiene, R. P., Siegel, D. A., & Nelson, N. B. (2003). Photolysis and the dimethylsulfide (DMS) summer paradox in the Sargasso Sea. *Limnology and Oceanography*, *48*(3), 1088–1100. https://doi.org/10.4319/lo.2003.48.3.1088

Vancoppenolle, M., Bopp, L., Madec, G., Dunne, J., Ilyina, T., Halloran, P. R., & Steiner, N. (2013). Future Arctic Ocean primary productivity from CMIP5 simulations: Uncertain outcome, but consistent mechanisms. *Global Biogeochemical Cycles*, *27*, 605–619. https://doi.org/10.1002/gbc.20055